Numerical Optimization and Map Construction of a Quadrupole Electromagnetic Actuated System

Zhijie Huan
Xiamen University of Technology
Weicheng Ma (jing11@mail.ustc.edu.cn)
Xiamen University of Technology
Quanchang Liao
Xiamen University of Technology
Zhenbo Peng
Xiamen University of Technology
Jiamin Wang
Xiamen University of Technology
Zhemin Zhang
Xiamen University of Technology

Research Article

Keywords: COMSOL, electromagnetic actuation, magnetic micro/nano particles

Posted Date: April 28th, 2021

DOI: https://doi.org/10.21203/rs.3.rs-454568/v1

Numerical Optimization and Map Construction of a Quadrupole Electromagnetic Actuated System

Zhijie Huan[1], Weicheng Ma[1,*], Quanchang Liao[1], Zhenbo Peng[1], Jiamin Wang[1], and Zhemin Zhang[1]

[1]School of Electrical Engineering and Automation, Xiamen University of Technology, Xiamen, 361024, China
[*]jing11@mail.ustc.edu.cn

ABSTRACT

Electromagnetic actuation is a new technique for non-invasive manipulation, which provides wireless and controllable power source for magnetic micro/nano particles. This technique shows great potential in the field of precise mechanics, environment protection and biomedical engineering. In this paper, a new quadrupole electromagnetic actuated system is constructed, this system is composed of four electromagnetic coils, each of the coil is actuated by an independent DC power supplier. The magnetic field distribution in the workspace is obtained through finite element modeling and numerical simulation via COMSOL, as well as the effect of the current flow through the coil in the field distribution. Moreover, parameters of the electromagnetic system are optimized through parametric modeling analysis. A magnetic field map is constructed for rapidly solving the desired driving current from the required magnetic flux density. The proposed work provides theoretical references and numerical fundamental for the control of magnetic particle in future.

Introduction

Micro-manipulation aims to control the movement and assembly of micro-particles in the target workspace for some specific application including micro-processing[1], environmental governance[2] and drug targeted delivery[3]. Since the size of the manipulated particle is in micro-scale, traditional embedded energy supply device is hard to be integrated directly. Thus, non-invasive mechanisms are introduced for micro-manipulation technology[4], including dielectrophoresis[5] generated by non-uniform electric field, optical tweezers[6] induced by focused laser beam, and magnetic driving force[7] generated by gradient magnetic field, etc. Compared with dielectrophoresis and optical tweezers, magnetic actuated technology has its advantages in biological compatibility and micro-flexibility[8,9], which has been widely investigated in recent years.

The actuators of magnetic actuated systems are usually composed of permanent magnets or electromagnetic coils. Permanent magnets have relatively high magnetic energy product per unit volume, which could generate large strength of magnetic field efficiently and economically[10]. However, the magnetic field induced by permanent magnet is difficult to be removed beyond the working state. The variation of the magnetic field could only be achieved by adjusting magnetic pole interval in the workspace[11]. The magnetic field generated by the electromagnetic coil could be controlled with variable currents flowing in the coils[12]. The electromagnetic system could provide a remote controllable driving force for magnetic particles in a relatively large workspace, which is convenient for system modeling and control law design[13]. Electromagnetic actuated system has been reported by many researchers. Kummer et al. introduced an electromagnetic driven system consisting of eight electromagnetic coils with iron cores, which can provide three dimensions of translation and two dimensions of rotation for magnetic particles in the workspace[14]. An electromagnetic driven system composed of two pairs of saddle coils with different geometric parameters was designed by Jeon et al.[15], which could enlarge the effective workspace for the manipulation. Li et al. proposed an electromagnetic actuated system with four intersecting electromagnetic coils in the plane. The end of the core near the workspace is designed as a probe, and the other end of the core is attached with a thin iron sheet[16]. This could not only increase generated magnetic field gradient, but also enlarge effective workspace. In this paper, quadrupole electromagnetic actuated system is proposed, which could provide real-time adjustable magnetic field distribution in its workspace with external programable current supplier. Parameters of the system are optimized through parametric modeling and finite element simulation. Moreover, based on the magnetic field data value of the discrete reference points, a magnetic field map in the workspace is constructed for obtaining the inverse solution of the required current value rapidly in real time. The proposed work provides a foundation for manipulation of micro-particles and improving the control response speed of the electromagnetic actuated system.

Results

System construction

A quadrupole electromagnetic actuated system is designed to generate a gradient magnetic field for manipulating of micro-particles. As shown in Figure 1, the basic structure of the system consists of four electromagnetic coils which is constituted by scaffold, copper coil and iron core. The coils are further connected to the power suppliers. Thus, a square magnetic workspace is provided in the center of the system.

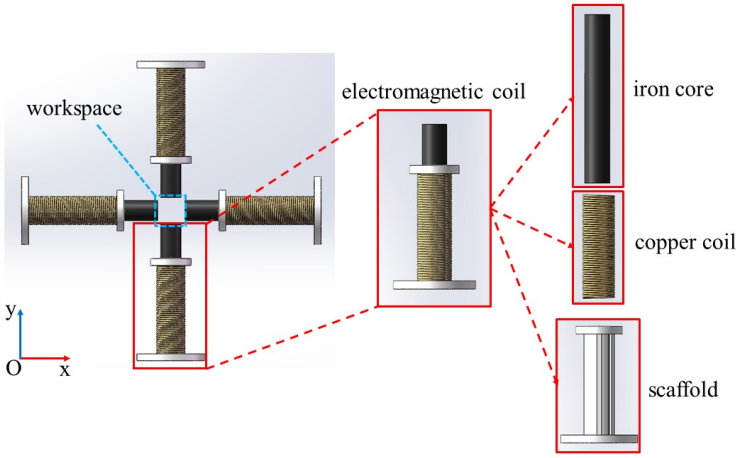

Figure 1. Combination of the electromagnetic coils and composition of a single coil.

As shown in Figure 2(a) and 2(b), the entire system is settled within an aluminum frame. Each electromagnetic coil is fixed with an adjustable supporter, as shown in Figure 2(c). As illustrated in Figure 2(d), the connection supporters consist of one H-type bracket and two guide rails. With these supporters, the relative distance of the four electromagnetic coils is alterable. Since the generated magnetic field is related to the structure of the system, the induced magnetic field could be further adjusted according to certain applications.

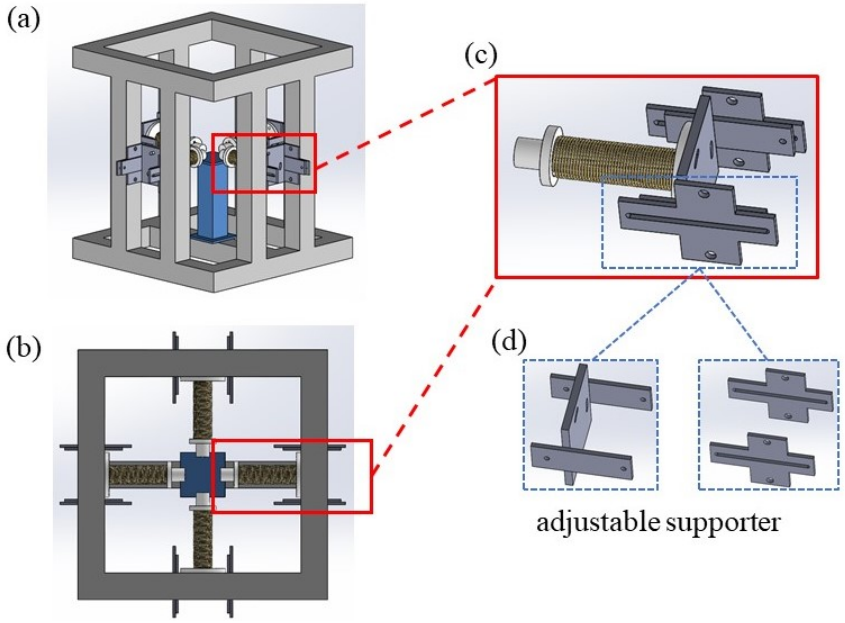

Figure 2. Configuration of the electromagnetic actuated system (a) structure of the entire system (b) top view of the system (c) fixation for the electromagnetic coils (d)adjustable supporter.

Simulation and Optimization

Parameter optimization

In order to evaluate and optimize the magnetic field distribution of the proposed electromagnetic system, a FEM model is constructed via the COMSOL software. The 3D model structure of the quadrupole magnetic system is firstly built in Solidworks. Four coils are aligned orthogonal to each other in X-Y plan, as shown in Figure 3(a). The model is then converted and imported into COMSOL for further analysis. Figure 3(b) illustrates the finite element grid division of the system within the software.

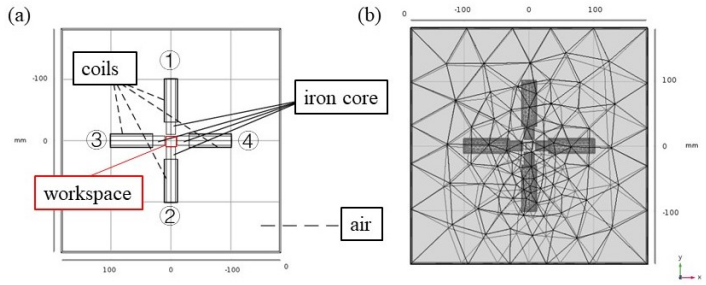

Figure 3. Finite element model of the electromagnetic actuated system (a) orthogonal structure (b) finite element grid division.

As given in equation 8, the magnetic field within the workspace could be calculated through the principle of vector superposition. Thus, the magnetic field generated by single coil is analyzed in the first place. According to the Biot-Savart law, the induced magnetic field is related to the design parameters of the electromagnetic coil system, such as, diameter of core, distance between coils and number of coils turns. Parameterized model of the system is built for optimization, as shown in Figure 4(a). In the simulation, coil 1 is applied with 1A current and there is no current going through the other coils. Magnetic field distribution in the central axis of coil one is exported. Simulation results within different parameters are illustrated in Figure 4(a-c).

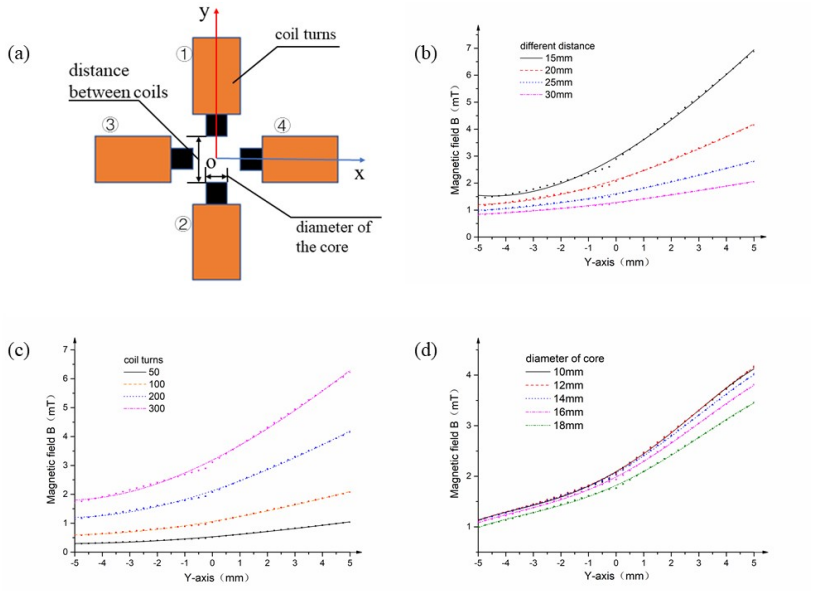

Figure 4. Parameter optimization of the electromagnetic system (a) parameterized model; (b) magnetic field distribution with different distance between coils; (c) magnetic field distribution with different coil turns; (d) magnetic field distribution with different diameters of iron core.

As illustrated in Figure 4(b), different distances between two concentric coils are set for the simulation. The distribution curves of magnetic field show that, the closer to the core the larger we get the gradient of magnetic field. Moreover, as the distance between two concentric coils increases, the magnetic field around the center of workspace and its gradient decrease obviously. For better driving characteristics, the distance between two concentric coils should be small enough. However, when we reduce the distance, the workspace would also be compressed. Thus, in order to guarantee a 10mm×10mm valid

workspace, 20mm is chosen as the distance between two concentric coils. The number of coil turns is also an important factor for magnetic field. The magnetic field distribution along Y-axis is analyzed with different coil turns, as shown in Figure 4(c). The magnetic field and its gradient could be enhanced as we increased the number of coils turns. This result could also be predicted theoretically from Equation (6). Nevertheless, the coils are spooled multi-layered for the limitation of size, which impedes the heat dissipation. To avoid excess thermal effect during long running operations, the number of coil turns is chosen as 200. Figure 4(d) summarized the magnetic field distribution with different diameters of iron core. As we reduce the diameters, the magnetic field and its gradient in the central axis gradually increase. A smaller iron core is preferred according to the simulation results. In addition, if the diameter of iron core is smaller than 10mm, the difficulty manufacturing and coil spooling process increased significantly. Overall consideration, the diameter of the iron core is set as 10 mm.

Magnetic field analysis

The parameters of the system are optimized along the central axis. In order to investigate the magnetic-field distribution in the workspace. The model is constructed according to Figure 3. After that, a current value of 1 A is applied to each electromagnetic coil. It should be noted that, the current is going in the opposite direction in coil 1 and coil 3, as well as in coil 2 and coil 4. While, current flow is in the same direction for coil 1 and coil 4. The magnetic field distribution in the 10 mm × 10 mm × 10 mm workspace could be calculated with finite element analysis. The three-dimensional steady state magnetic field distribution is proposed in Figure 5(a). In order to show more details, the magnetic field distributions in two-dimensional cross section are exported in Figure 5(b-d). It is evident that, the magnetic field in each 2D plane is symmetrical distributed. As illustrated in Figure 5(b), the magnetic field strength near the coils with opposite currents are much higher compared with the rest region. As we could observed from Figure 5(c) and 5(d), the field strength decreased along the Z-axis significantly. After the simulation, we

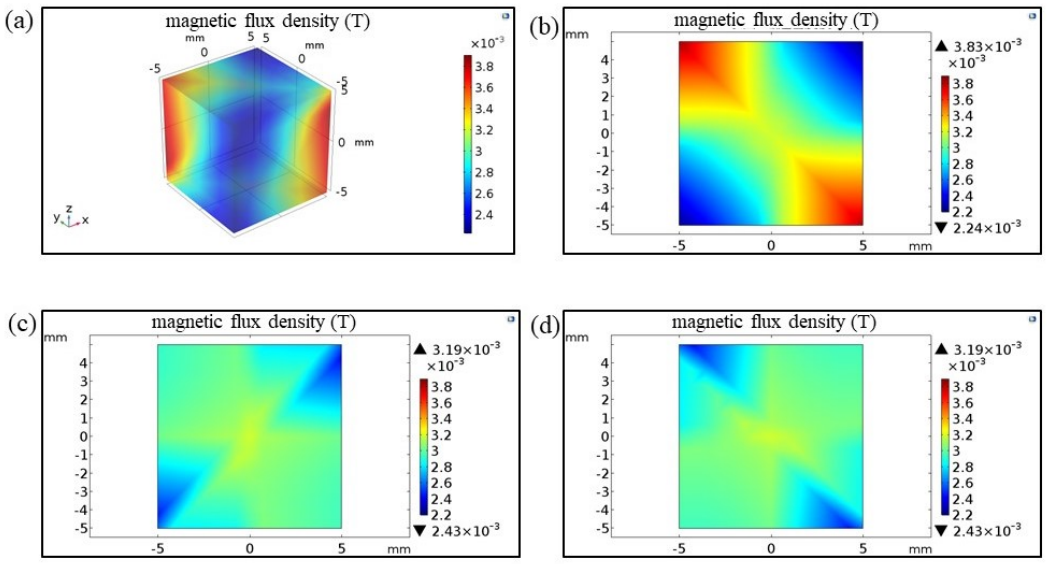

Figure 5. Simulation of the electromagnetic system in the workspace (a) 3D magnetic field distribution; (b) magnetic field distribution in XY-plane; (c) magnetic field distribution in XZ-plane; (d) magnetic field distribution in YZ-plane.

reconstructed the system with optimized parameters. A Gaussmeter (LZ-610) is used to measure the magnetic field distribution along the central axis of coil 1, which is applied with a current of 1 A. The probe of the gaussmeter is installed on a triaxial micromotion platform, the value is recorded with distance interval of 0.5 mm. Figure 6 shows the comparison between results from software simulation and real measurement for coil 1. The comparison result shows that simulation results are consistent with the experimental results. Some minor error could be introduced by the system disturbance and manufacturing process.

Magnetic field map construction

According to equation 6 and 7, during the manipulation of micro-particle, the applied current could be calculated from the required driving force, which is given by the control algorithm. However, partial differential equations should be solved in this process and the solution is non-unique. The complex solution process could introduce delay for the manipulation. One possible solution is to prepare a magnetic field database for the workspace, with which we could find out the certain current directly from the given magnetic field strength. As illustrated in equation 7, the magnetic flux density is in direct proportion

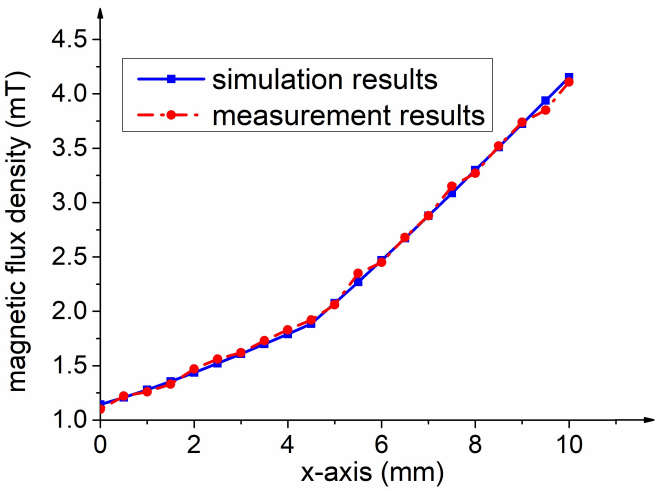

Figure 6. Comparison between magnetic field evaluated with COMSOL and measured with gaussmeter in X-axis.

to the applied current. Furthermore, the overall magnetic field depends on the vector superposition of each electromagnetic coils' contribution. So we just need to construct the a unit-current magnetic field map for each coils. In order to construct the unit-current magnetic field map, the values of the magnetic flux density for each node in FEM model are exported from COMSOL. The discrete reference points are treated as the data source. During the manipulation, the target particle could be anywhere in the workspace whose position is captured from the visual system. To determine magnetic flux density in the target position, spherical search method and inverse distance weighting algorithm are utilized. For an arbitrary point in the workspace, a spherical region with variable diameter is used for searching the data sample around the target. The diameter is an auto-increment value ensuring finding enough neighboring sample data. The mechanism is shown in Figure 7.

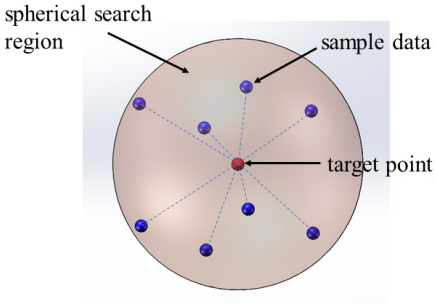

Figure 7. magnetic field map establishment process.

The magnetic flux density in target position could be given as:

$$\vec{B_0} = \sum_{a=x,y,z} \vec{B_{0a}} \tag{1}$$

where, B_{0a} is target magnetic flux density in X-axis, Y-axis, and Z-axis, respectively. The value of each axis could be fitted by the distance inverse weight method. The interpolation weights are set as reciprocal of distance between the target point and the sample data points.

$$B_{0a} = \frac{\sum_{i=1}^{n} \frac{1}{d_{ia}} B_{ia}}{\sum_{i=1}^{n} \frac{1}{d_{ia}}} \tag{2}$$

where, B_{ia} is the magnetic flux density in certain axis of sample data point.

As illustrated in Figure 8, a simple magnetic flux density fitting system is developed as the database of magnetic field. When we set the coordinate of the target point, the magnetic flux density could be fitted according to the numbers of reference data points.

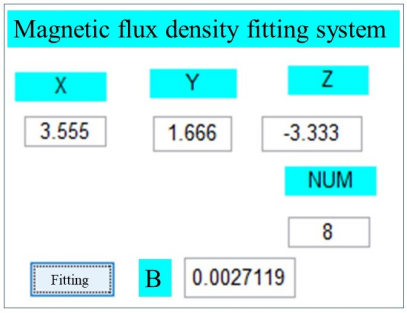

Figure 8. simple magnetic flux density fitting system.

Micro-particle manipulation

Experiments were performed with the proposed system to manipulate magnetic micro-particle. A simple PID controller was used to manipulate the microparticle tracking desired trajectory. The radius of the microparticle is 5 μm with a density of $1.1 g/cm^3$. During the manipulation, the microparticle was suspended in salt water which has a similar density to avoid sinking or rising. Figure 9 illustrates the captured images for manipulating a microparticle along desired circular path, in 5s, 25s, and 45s, separately.

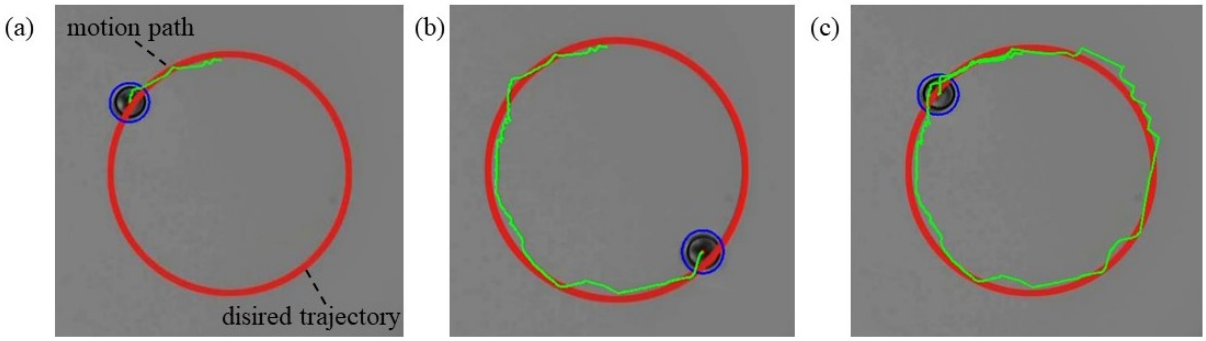

Figure 9. micro-particle manipulated with the proposed system along a circular path.(a)image captured in 5s; (b)image captured in 25s; (c)image captured in 45s

Discussion

A quadrupole electromagnetic actuated system is presented to generate a gradient magnetic field for manipulating of micro-particles. The overall structure of the system is constructed. The magnetic field distribution is simulated with COMSOL. Furthermore, parameters of the electromagnetic coils are optimized for enhancing the magnetic flux density within the workspace. The magnetic field map of the workspace is constructed via spherical search method and inverse distance weighting algorithm. The proposed system was utilized to manipulate the microparticle along a preset circular path. This work provides theoretical references and numerical fundamental for the control of magnetic particle. Future work would focus on the control method of the micro-particle manipulation with this electromagnetic actuated system.

Methods

System construction

In order to enhance the induced magnetic field, DT4-core is utilized for the electromagnetic coils which has excellent electromagnetic performance. Meanwhile, the characteristic of electrical pure iron DT4 is also friendly with manufacturing and

could be fabricated according to the designed structure easily. The B-H curve of DT4 is given in Figure 10. The DT4-core has a large area of liner part which could be used for our electromagnetic system. Detailed electromagnetic parameter of DT4 is listed in Table 1. As illustrated, DT4 has relatively low coercive force and high magnetic conductivity which benefits the generation of precise magnetic field.

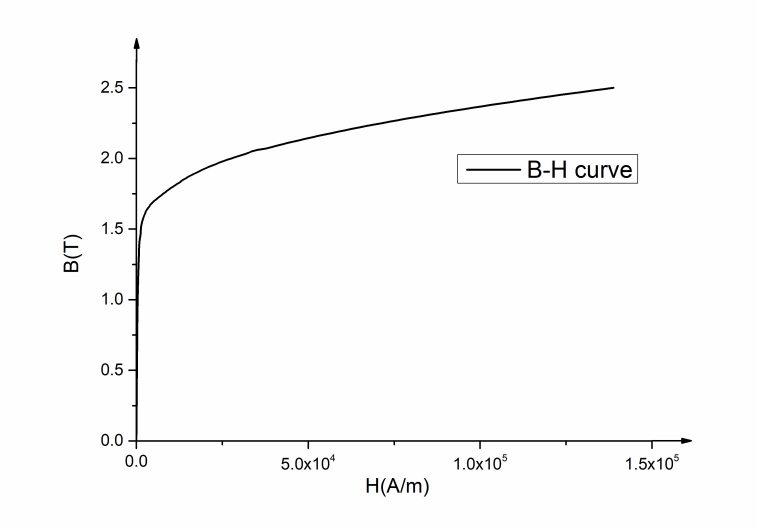

Figure 10. B-H curve of DT4.

Material	Coercive Force (Hc)	Magnetic Conductivity (μ)
DT4	$\leq 96A/m$	$\geq 7.5H/m*10^{-3}$

Table 1. Main electromagnetic parameters of DT4.

To avoid electromagnetic interference, the entire setup is settled on a nonmagnetic optical vibration isolation platform, as shown in Figure 11. A commercial 3D printer (M3D) is used to fabricate the core-scaffold with standard PLA filaments. The 3D models of scaffold are first built with Solidworks. Each scaffold is designed with several grooves along the axial direction for promoting heat dissipation of coils during operating process. Enameled copper wires are wrapped and stacked around the scaffold forming electromagnetic coils, with a diameter of 1.3 millimeters. The electromagnetic coils are fixed on the aluminum profile bracket constituting a quadrupole electromagnetic system. An aluminum stage is installed right under the workspace which could be used for placing the experimental chip. The observation system is composed of optical microscope, CCD camera and computer, in order to record the movement of micro-particles. Programmable power suppliers are connected to each coil to control the current input of the manipulation system.

Electromagnetic actuation mechanism

As a magnetic microparticle suspended in the gradient magnetic field, both force and torque will be induced on the particle related to the magnetic property of microparticles and the distribution of the magnetic field. The induced force and torque could be obtained from the equations:

$$\vec{F} = \left(\vec{Q} \bullet \nabla\right) \vec{B} \tag{3}$$

$$\vec{T} = \vec{Q} \times \vec{B} \tag{4}$$

where, $\vec{B} = (B_x, B_y, B_z)^T$ is the magnetic flux density of the magnetic field in Cartesian coordinate system, $\vec{Q} = (Q_x, Q_y, Q_z)^T$ is the magnetic moment of the magnetic particle,∇ is the gradient operator. For a liner, isotropic, and homogeneous magnetic particle with the volume V_p and the susceptibility χ, the magnetic moment $\vec{Q}$ could be defined as:

$$\vec{Q} = V_p \frac{\chi}{\mu_0 (1+\chi)} \vec{B} \tag{5}$$

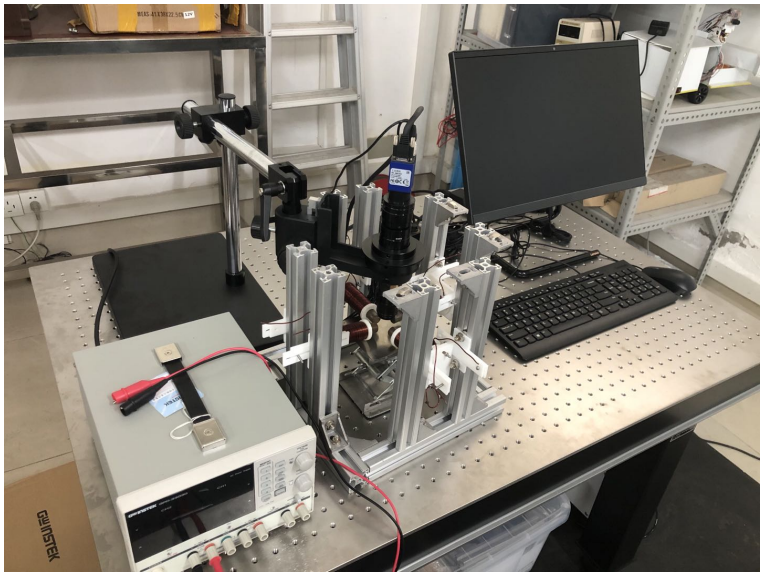

Figure 11. The electromagnetic actuated system setup.

where, $\mu_0 = 4\pi \times 10^{-7}\ Tm/A$ is the free-space permeability. Substituting equation 5 into equation 3, the magnetic force could be written as:

$$\vec{F} = V_p \frac{\chi}{\mu_0 (1+\chi)} \left(\vec{B} \bullet \nabla\right) \vec{B} \tag{6}$$

Since the magnetic field of the electromagnetic coils is generated by current-carrying coils, the magnetic flux density could be calculated with the Biot-Savart law. With current $\vec{I}$, the induced magnetic flux density could be given as:

$$\vec{B} = \frac{\mu_0 I}{4\pi} \int \frac{d\vec{l} \times \left(\vec{P} - \vec{P}'\right)}{\left|\vec{P} - \vec{P}'\right|^3} = \vec{\zeta}_B I \tag{7}$$

where,$\vec{P} = [p_x, p_y, p_z]^T$ is the position of the manipulated microparticle. $\vec{P}'$ is the magnetic field source position. $d\vec{l}$ is the current element in the magnetic coils. $\vec{\zeta}_B = \frac{\mu_0}{4\pi} \int \frac{d\vec{l} \times \left(\vec{P} - \vec{P}'\right)}{\left|\vec{P} - \vec{P}'\right|^3}$ is related to the position of the particle. According to equation 6 and 7, the magnetic force induced on the microparticle placed in the magnetic field is related to the coil current $\vec{I}$ and the particle position $\vec{P}$. Generated magnetic field for a certain magnetic coil is linearly related to the coil current, which could be obtained from equation 7. As we have four electromagnetic coils, the magnetic field in position $\vec{P}$ is a vector superposition of each coil's contribution, which could be written as:

$$\vec{B}_p(x,y,z) = \sum_{n=1}^{4} \vec{B}_{np}(x,y,z) = \sum_{n=1}^{4} \left(\vec{\zeta}_{nB} I_n\right) \tag{8}$$

where, $\vec{B}_{np}(x,y,z)$ is the contribution in position $\vec{P}$ of any one electromagnetic coil, I_n is the current input of the magnetic coil, separately.

References

1. Li, J. *et al.* Self-propelled nanomotors autonomously seek and repair cracks. *Nano Lett.* **15**, 7077–7085 (2015).

2. Wang, B. *et al.* Bioinspired superhydrophobic fe3o4@ polydopamine@ ag hybrid nanoparticles for liquid marble and oil spill. *Adv. Mater. Interfaces* **2**, 1500234 (2015).

3. Gao, C. *et al.* Stem cell membrane-coated nanogels for highly efficient in vivo tumor targeted drug delivery. *Small* **12**, 4056–4062 (2016).

4. Meng, K. *et al.* Motion planning and robust control for the endovascular navigation of a microrobot. *IEEE Transactions on Ind. Informatics* **16**, 4557–4566 (2019).

5. Chu, H., Huan, Z., Mills, J., Yang, J. & Sun, D. Three-dimensional cell manipulation and patterning using dielectrophoresis via a multi-layer scaffold structure. *Lab on a Chip* **15**, 920–930 (2015).

6. Cheah, C. C., Li, X., Yan, X. & Sun, D. Observer-based optical manipulation of biological cells with robotic tweezers. *IEEE Transactions on Robotics* **30**, 68–80 (2013).

7. Ma, W., Li, J., Niu, F., Ji, H. & Sun, D. Robust control to manipulate a microparticle with electromagnetic coil system. *IEEE Transactions on Ind. Electron.* **64**, 8566–8577 (2017).

8. Pankhurst, Q. A., Connolly, J., Jones, S. K. & Dobson, J. Applications of magnetic nanoparticles in biomedicine. *J. physics D: Appl. physics* **36**, R167 (2003).

9. Ma, W., Xu, M., Zhong, Z., Li, X. & Huan, Z. Closed-loop control for trajectory tracking of a microparticle based on input-to-state stability through an electromagnetic manipulation system. *IEEE Access* **8**, 46537–46545 (2020).

10. Mahoney, A. W. & Abbott, J. J. Generating rotating magnetic fields with a single permanent magnet for propulsion of untethered magnetic devices in a lumen. *IEEE Transactions on Robotics* **30**, 411–420 (2013).

11. Wright, S. E., Mahoney, A. W., Popek, K. M. & Abbott, J. J. The spherical-actuator-magnet manipulator: A permanent-magnet robotic end-effector. *IEEE Transactions on Robotics* **33**, 1013–1024 (2017).

12. Yesin, K. B., Vollmers, K. & Nelson, B. J. Modeling and control of untethered biomicrorobots in a fluidic environment using electromagnetic fields. *The Int. J. Robotics Res.* **25**, 527–536 (2006).

13. Wang, X. *et al.* A three-dimensional magnetic tweezer system for intraembryonic navigation and measurement. *IEEE Transactions on Robotics* **34**, 240–247 (2017).

14. Kummer, M. P. *et al.* Octomag: An electromagnetic system for 5-dof wireless micromanipulation. *IEEE Transactions on Robotics* **26**, 1006–1017 (2010).

15. Jeon, S., Jang, G., Choi, H. & Park, S. Magnetic navigation system with gradient and uniform saddle coils for the wireless manipulation of micro-robots in human blood vessels. *IEEE transactions on magnetics* **46**, 1943–1946 (2010).

16. Li, D., Niu, F., Li, J., Li, X. & Sun, D. Gradient-enhanced electromagnetic actuation system with a new core shape design for microrobot manipulation. *IEEE Transactions on Ind. Electron.* **67**, 4700–4710 (2019).

Acknowledgements

Funding for this research was provided by National Natural Science Foundation of China (No.61903315 and No.62003285) , and the Natural Science Foundation of Fujian Province (No.2019J05124 and No.2019J01869), and the grant from Scientific Research Projects for Overseas Students in Xiamen (No.2018-310 and No.2019-232).

Author contributions statement

Z.H. performed experiments, and wrote the paper, Q.L. conducted the simulation work, Z.P. constructed the setup device, Z.H. and W.M. analysed the results. J.W. and Z.Z. revised the manuscript. All authors reviewed the manuscript.

Figures

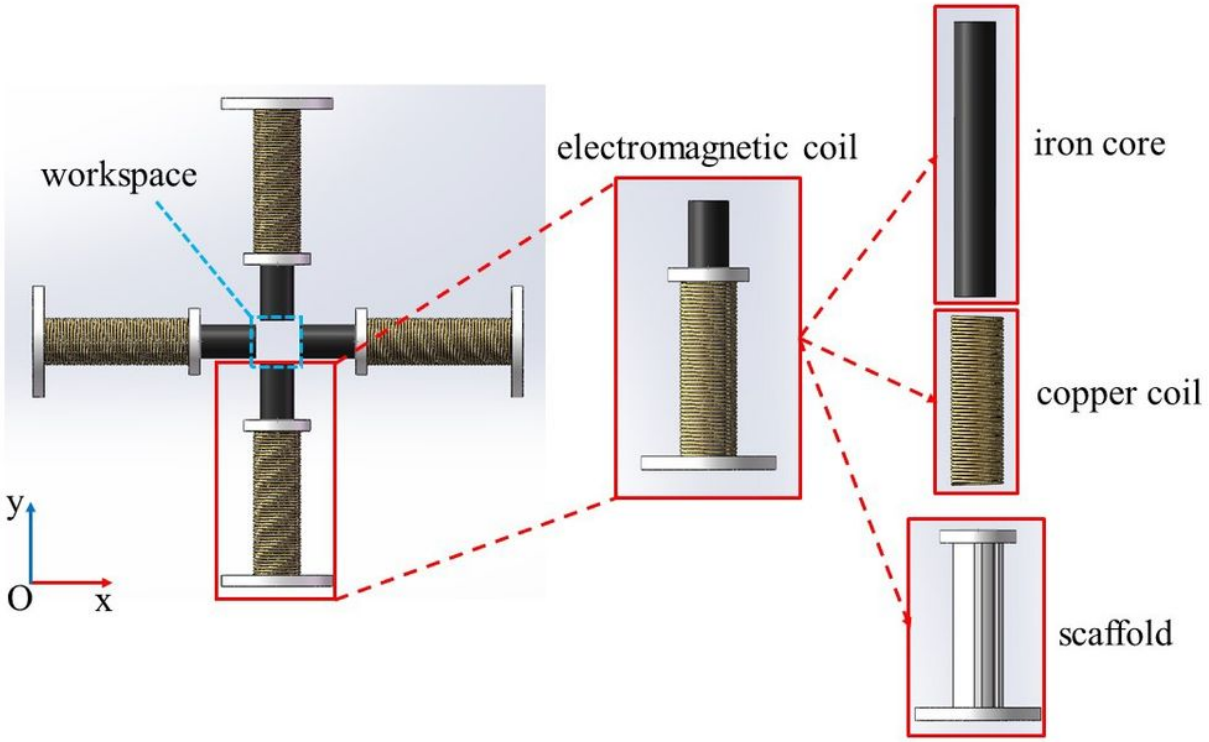

Figure 1

Combination of the electromagnetic coils and composition of a single coil.

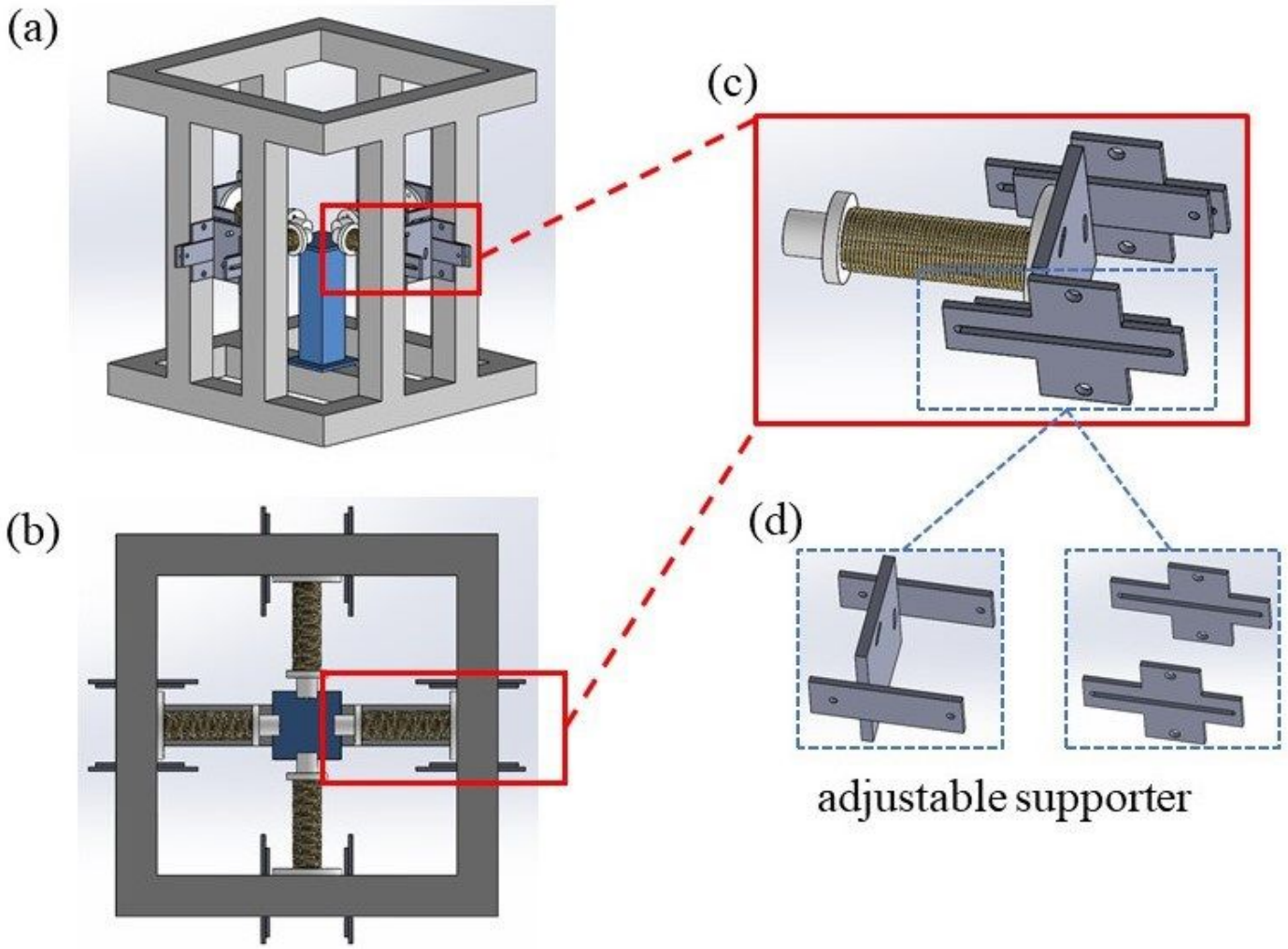

Figure 2

Configuration of the electromagnetic actuated system (a) structure of the entire system (b) top view of the system (c) fixation for the electromagnetic coils (d)adjustable supporter.

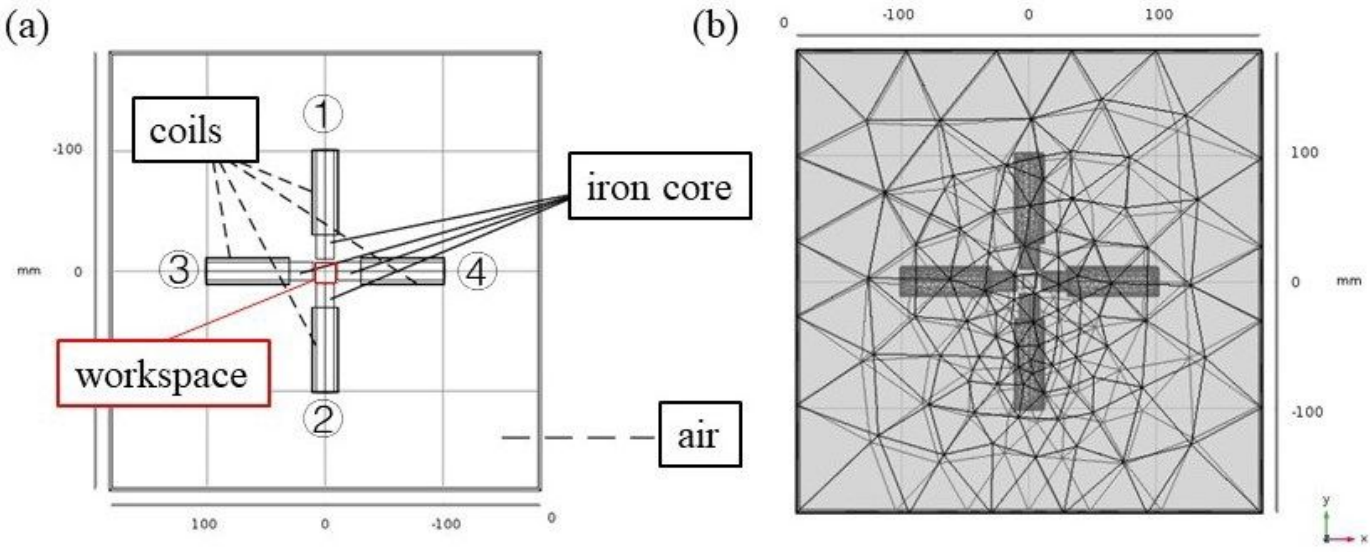

Figure 3

Finite element model of the electromagnetic actuated system (a) orthogonal structure (b) finite element grid division.

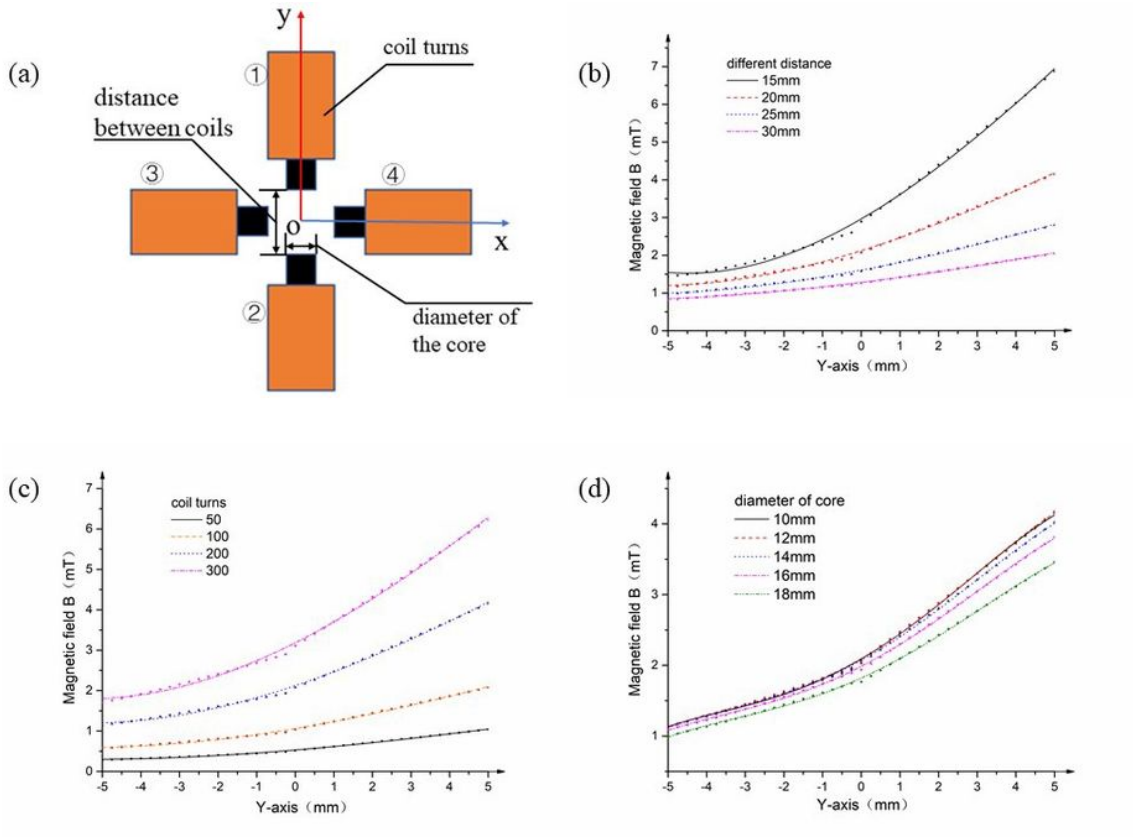

Figure 4

Parameter optimization of the electromagnetic system (a) parameterized model; (b) magnetic field distribution with different distance between coils; (c) magnetic field distribution with different coil turns; (d) magnetic field distribution with different diameters of iron core.

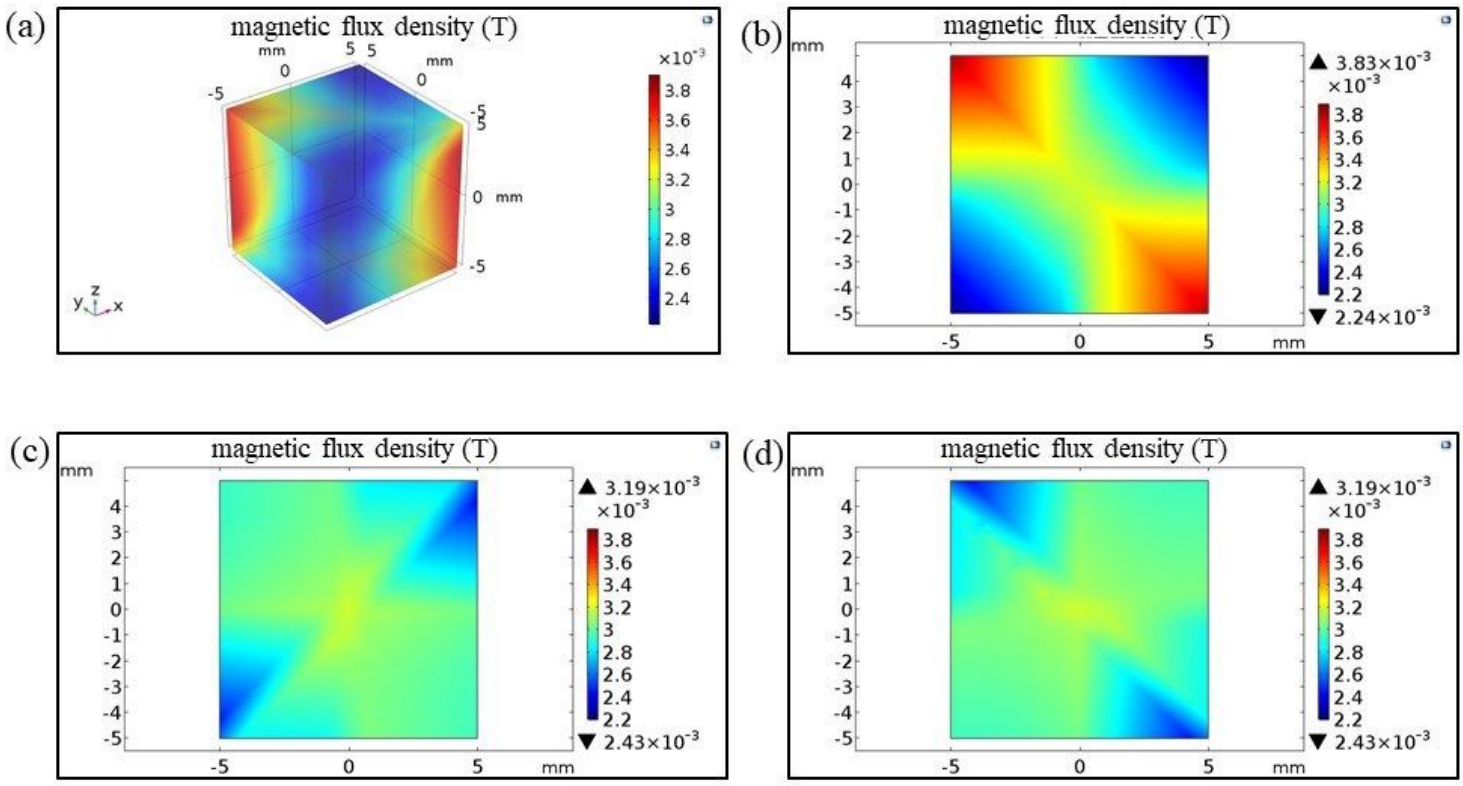

Figure 5

Simulation of the electromagnetic system in the workspace (a) 3D magnetic field distribution; (b) magnetic field distribution in XY-plane; (c) magnetic field distribution in XZ-plane; (d) magnetic field distribution in YZ-plane.

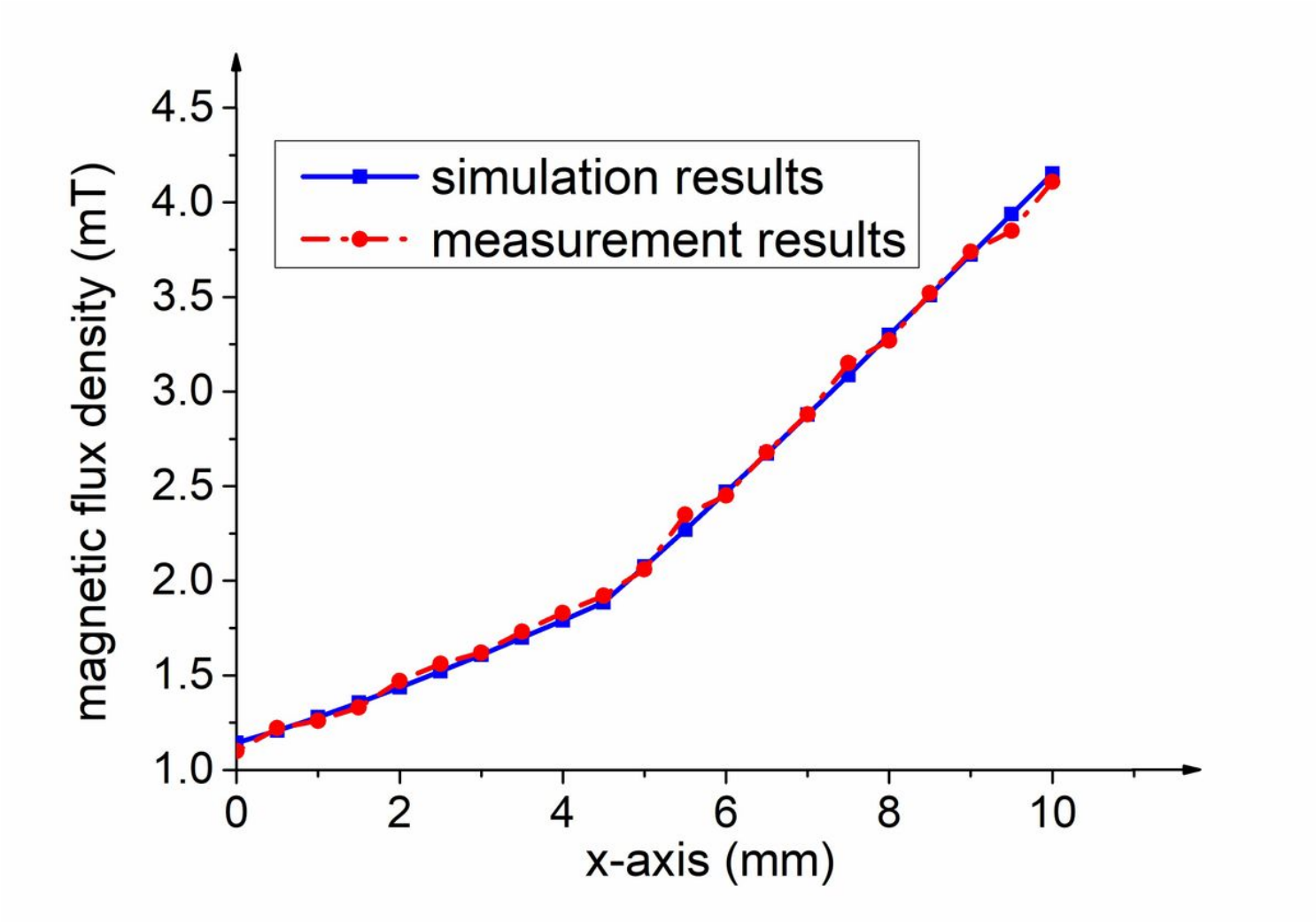

Figure 6

Comparison between magnetic field evaluated with COMSOL and measured with gaussmeter in X-axis.

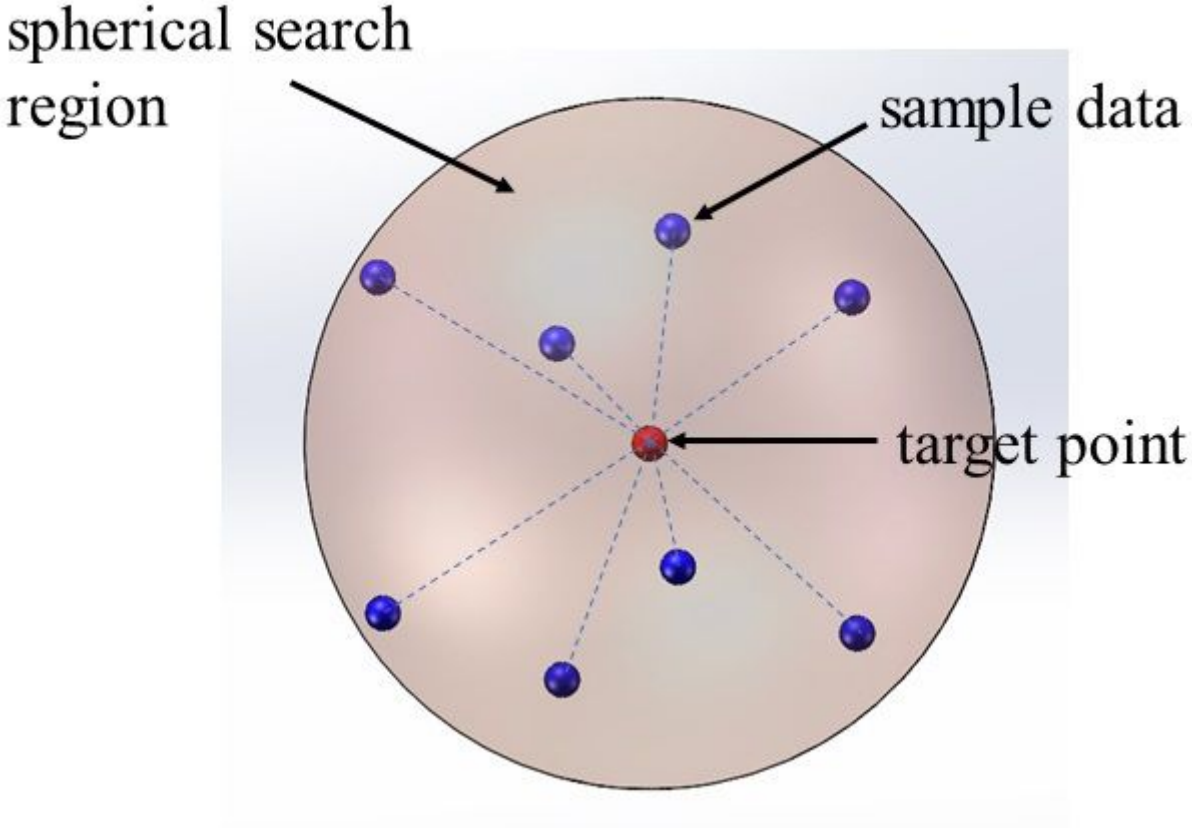

Figure 7

magnetic field map establishment process.

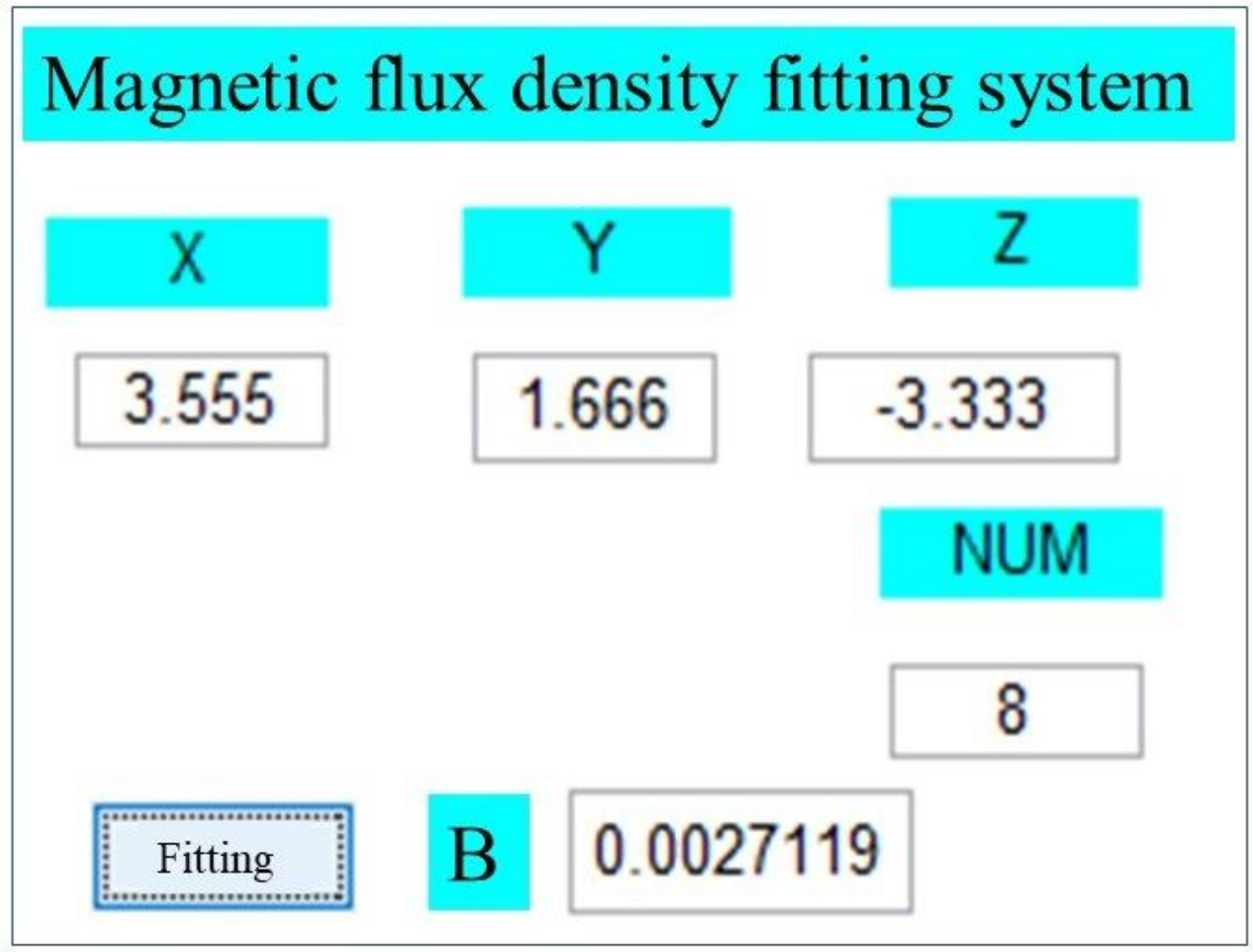

Figure 8

simple magnetic flux density fitting system.

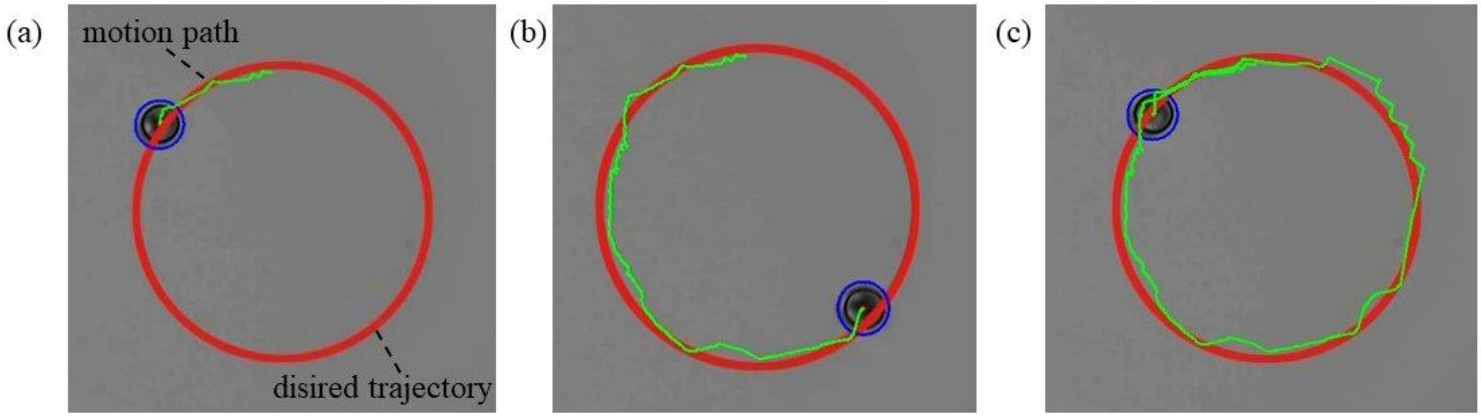

Figure 9

micro-particle manipulated with the proposed system along a circular path.(a)image captured in 5s; (b)image captured in 25s; (c)image captured in 45s

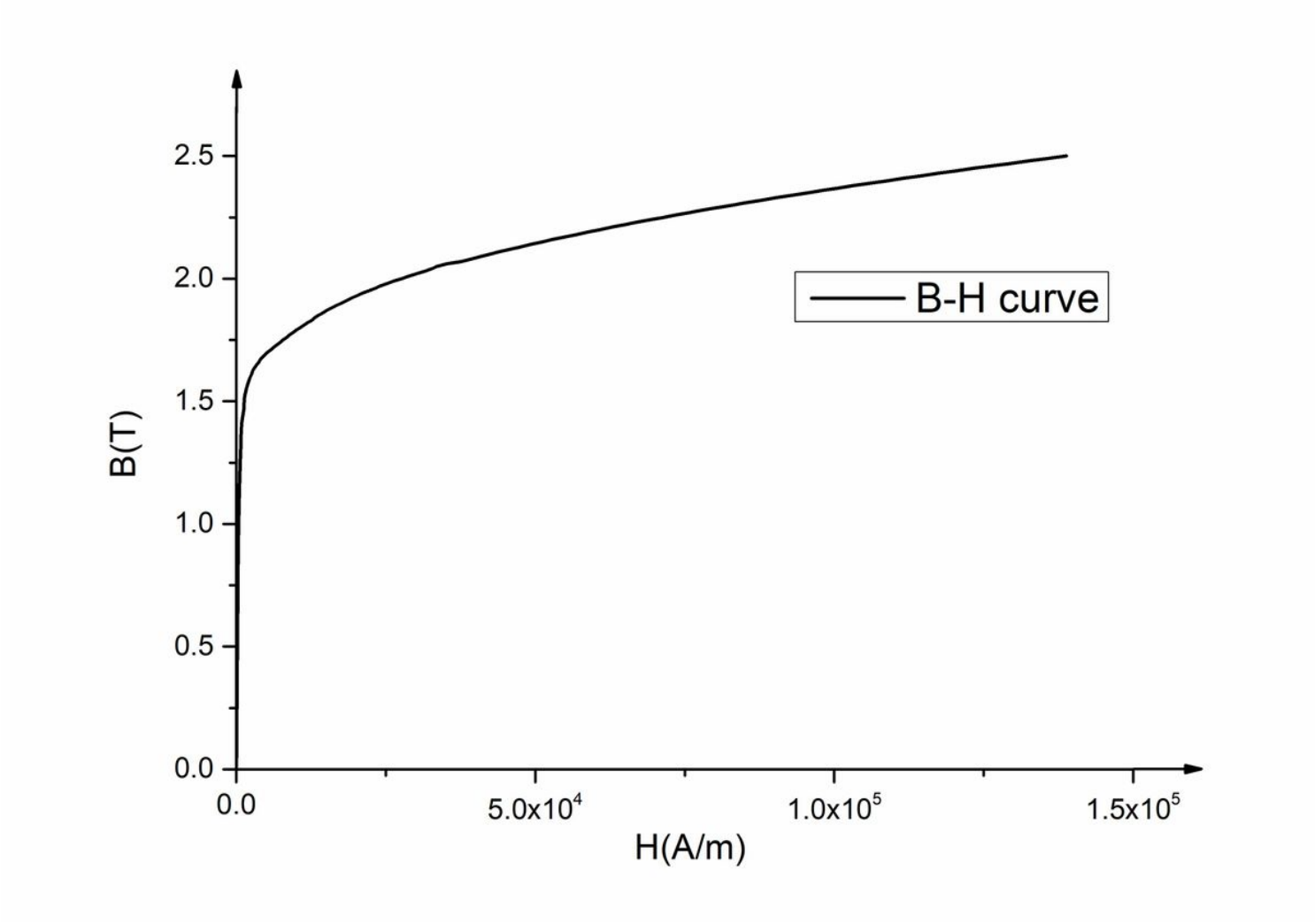

Figure 10

B-H curve of DT4.

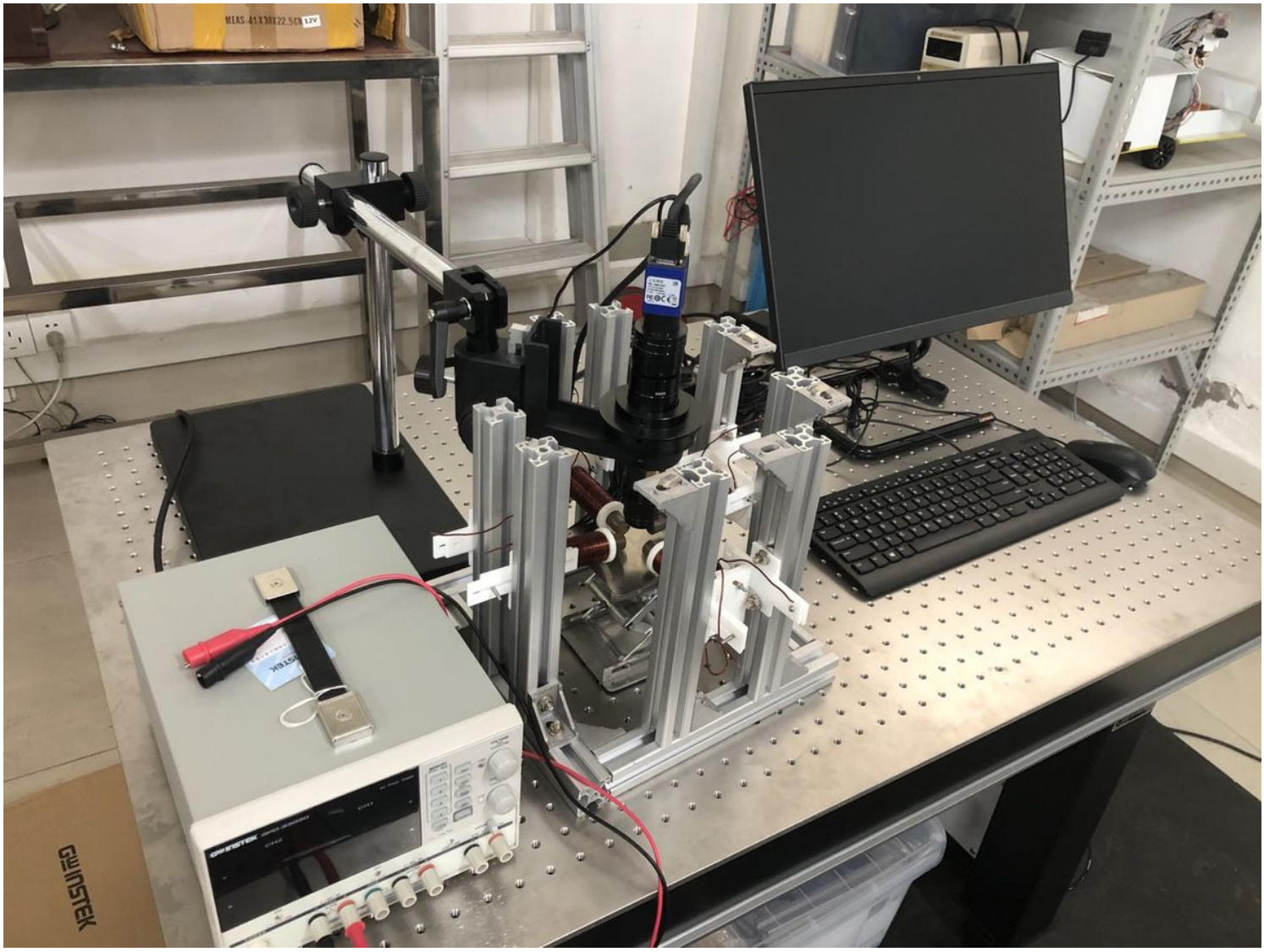

Figure 11

The electromagnetic actuated system setup.